



Electrochemical Microbiosensor for Detecting COVID-19 in a Patient Sample Based on Gold Microcuboids Pattern

Waleed A. El-Said¹ · Abdullah S. Al-Bogami¹ · Wael Alshitari¹ · Deia A. El-Hady¹ · Tamer S. Saleh¹ · Mohamed A. El-Mokhtar² · Jeong-Woo Choi³

Received: 6 April 2021 / Revised: 14 June 2021 / Accepted: 18 June 2021 / Published online: 9 August 2021
© The Korean BioChip Society 2021

Abstract

As continues increasing the COVID-19 infections, there is an urgent need for developing fast, simple, selective, and accurate COVID-19 biosensors. A highly uniform gold (Au) microcuboid pattern was used as a microelectrode that allowed monitoring a small analyte. The electrochemical biosensor was used to monitor the COVID-19 S protein within a concentration range from 100 to 5 pmol L⁻¹; it showed a lower detection limit of 276 fmol L⁻¹. Finally, the developed COVID-19 sensor was used to detect a positive sample from a human patient obtained through a nasal swab; the results were confirmed using the PCR technique. The results showed that the SWV technique showed high sensitivity towards detecting COVID-19 and good efficiency for detecting COVID-19 in a positive human sample.

Keywords COVID-19 · Gold microelectrode · Cyclic voltammetry · Square wave voltammetry · Electrochemical biosensor · Raman spectroscopy · Nasal swab

1 Introduction

More than 30 strains of coronavirus were identified, including HCoV-229E, HCoV-OC43, SARS-CoV, HCoV-NL63, HCoV-HKU1, and MERS-CoV [1]. In addition, a novel coronavirus (COVID-19) has reported at the end of 2019, which has fast spread worldwide in a short time compared with other coronaviruses [2–6]. Thus, there is an urgent need to find antiviral drugs besides developing an accurate, simple, and sensitive sensing method. However, the early diagnosis is difficult because there are no initial characteristic symptoms of COVID-19 in the early stage of infection; besides, many cases did not show the usual signs [7].

The PCR assay is the golden technique for COVID-19 detection; however, the high cost, needing specialist laboratories, skilled persons, and consuming a long time are the main challenges for its widely uses [8, 9]. On the other hand, the enzyme-linked immunosorbent assay (ELISA) was used to detect the receptor protein using the corresponding antibody [10, 11]. Thus, it is of great urgency to develop rapid, reproducible, cost-effective, easy-to-use, accurate, sensitive, and selective assays for the early diagnosis of COVID-19 in different specimens.

Biosensors possess many advantages, including the fast response and the high selectivity towards several biological species. Electrochemical-based biosensors are among the most widely used, simple, accurate, prompt, and sensitive detecting assays of biomarkers without any pretreatments with a very low detection limit (LOD) [11–13]. Nanomaterials (e.g., gold and silver) were reported to modify the traditional electrodes to develop highly sensitive and selective electrochemical sensors [14–22].

We reported developing a sensitive and selective COVID-19 electrochemical biosensor using a highly uniform Au micropattern to improve the electrochemical conductivity. The anti-COVID-19 antibodies were used as probes for monitoring the COVID-19 based on cyclic voltammetry (CV) and square wave voltammetry (SWV) techniques. The

✉ Waleed A. El-Said
waahmed@uj.edu.sa

✉ Jeong-Woo Choi
jwchoi@sogang.ac.kr

¹ Department of Chemistry, College of Science, University of Jeddah, P.O. Box 80327, Jeddah 21589, Saudi Arabia

² Department of Microbiology and Immunology, Faculty of Medicine, Assiut University, Assiut 71515, Egypt

³ Department of Chemical and Biomolecular Engineering, Sogang University, 35 Baekbeom-Ro, Mapo-Gu, Seoul 04107, Republic of Korea

developed biosensor showed the capability to detect the COVID-19 protein over a wide range of concentrations from 5 nmol L^{-1} to 100 pmol L^{-1} with a LOD of 276 fmol L^{-1} SWV technique. Furthermore, we have used this biosensor to detect the COVID-19 in a real human sample obtained from the nasal swab, which confirmed the capability of this electrochemical biosensor for real uses for detecting the COVID-19 without any sample preparations.

2 Results and Discussion

2.1 Characterization of the Au Micropattern Substrate

Figure 1a showed a schematic diagram of the COVID-19 electrochemical biosensor based on CV and SWV techniques. The sensor is composed of Au microcuboid pattern-coated PDMS as microelectrode. Firstly, we immobilized the

anti-COVID-19 antibody onto the Au microcuboid pattern was used it as a specific probe for COVID-19 S protein to capture the COVID-19 protein. Furthermore, the Au microcuboid pattern would improve the electrochemical conductivity and analyze a small target analyte. Next, the SEM image was used to investigate the morphology of the Au micropattern substrate that indicated the highly uniform distribution of the Au cuboid structures with a length of about $1.47 \mu\text{m}$ and a width of about 730 nm as shown in Fig. 1b. Furthermore, the topography of this substrate was studied using the AFM technique, which showed the fabrication of a uniform microcuboid pattern with a length of about $1 \mu\text{m}$ and a width of about 500 nm (Fig. 1c).

2.2 Electrochemical Detection of COVID-19 Protein

The direct immobilization of $50 \mu\text{M}$ of anti-COVID-19 antibody onto the Au cuboid microcuboid was confirmed using Raman spectroscopy. The SERS spectrum of the

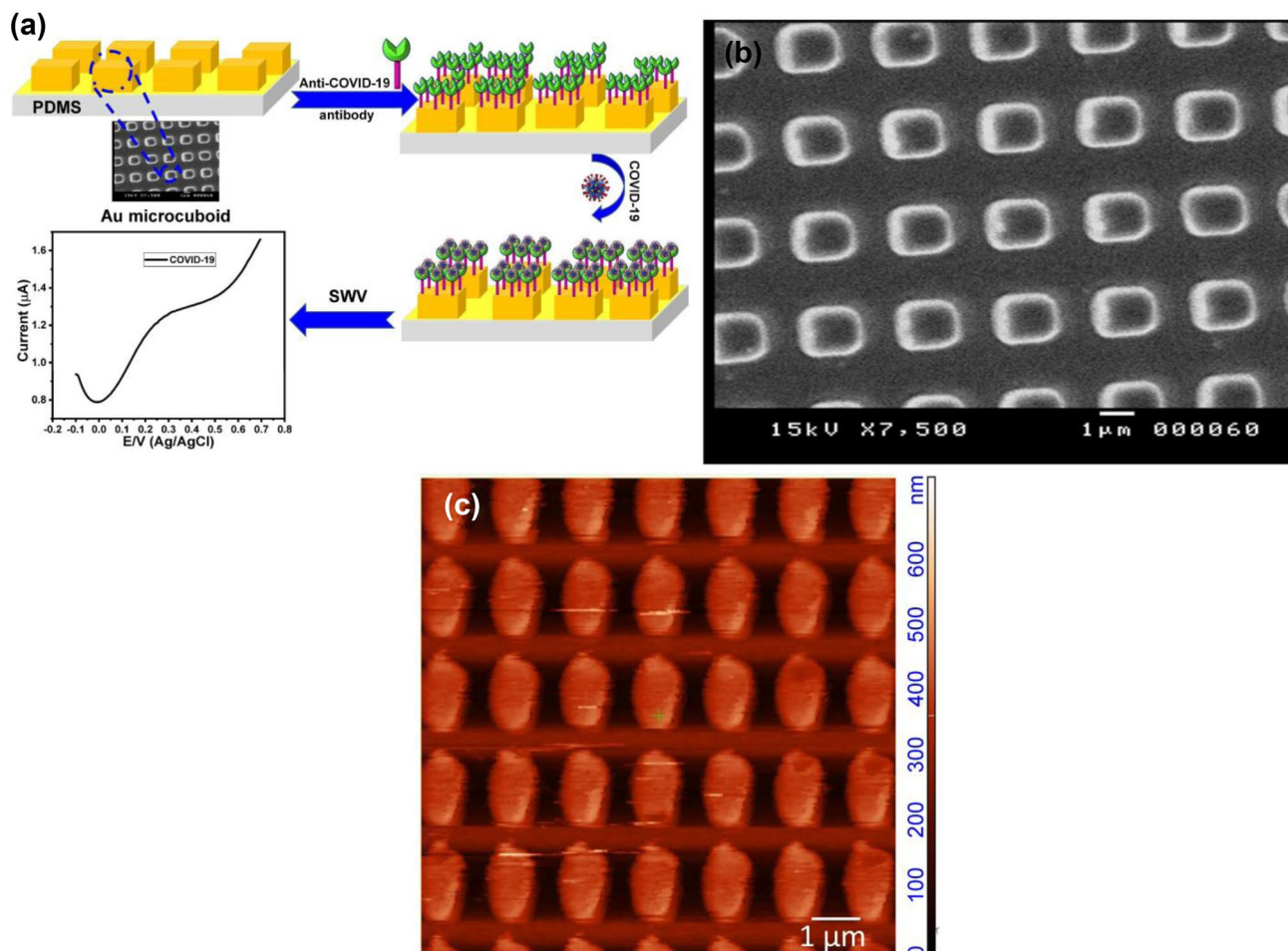


Fig. 1 a Schematic diagram of electrochemical COVID-19 microbiosensor that including, (i) immobilization of antiCOVID-19 antibody, and (ii) capturing of COVID-19 protein (not real scale), **b** SEM

image of Au microcuboid structures, scale bar $1 \mu\text{m}$ and (c) AFM topography of the Au microcuboid structures, scale bar 500 nm

anti-COVID-19 antibody was represented in Fig. 2a, which showed a set of SERS peaks located at 541 cm⁻¹ (S–S bond of protein), 635 cm⁻¹ (Tyr: C–C twisting), 936 cm⁻¹ (α-helix, str. C–C, str. C–N), 1070 cm⁻¹ (str. C–N in protein, phenylalanine), 1189 cm⁻¹ (tryptophan, phenylalanine, str. C–N and bending N–H of Amide III), 1318 cm⁻¹ (α-helix, Amide III), and 1444 cm⁻¹ (Amide II/N–H bending, C–N stretch, bending CH₂ of proteins) [23–28].

The COVID-19 biosensor was fabricated by interacting a 50 μL of the COVID-19 protein with an anti-COVID-19 antibody/Au microcuboid pattern. Figure 2b showed the SERS spectra of the anti-COVID-19 antibody/Au microcuboid substrate before and after the interaction with the COVID-19 protein, which exhibited a set of new SERS signals. The characteristics SERS signals including peaks at 526 cm⁻¹ (S–S), 655 cm⁻¹ (tryptophan, sidechain/indole ring modes), 770 cm⁻¹ (tryptophan, sidechain/indole ring modes), 927 cm⁻¹ (α-helix, Backbone skeletal stretch/C–C, C–N stretches), 1032 cm⁻¹ (phenylalanine, sidechain/phenyl ring modes), 1144 cm⁻¹ and 1185 cm⁻¹ (tyrosine and phenylalanine, sidechain/indole ring mode), 1320 cm⁻¹ (α-helix, Amide III/C–N stretch, N–H deformation), 1420 cm⁻¹

(Symmetric COO⁻ stretch), 1456 cm⁻¹ (Amide II/N–H bending, C–N stretch), 1544 cm⁻¹ and 1586 cm⁻¹ (tryptophan, Amide II/indole ring mode), and 1676 cm⁻¹ (β-sheet, Amide I/C=O stretch).

After confirmation of the capture of COVID-19 protein by anti-COVID-19 anti-body immobilized on Au microcuboid electrode (Fig. 2b), the CV response of the substrate was investigated before and after immobilization of the COVID-19 protein. Figure 2c showed the cyclic voltammogram of the bare Au microcuboid electrode that represented a background without any redox peaks. The CV response of the an-ti-COVID-19 antibody/Au microcuboid electrode was investigated in Fig. 2d, which indicated two redox peaks, a cathodic peak at about 0.0 V and a weak and broad oxidation peak. Thus, it is difficult to determine the oxidation potential peak. Figure 2e showed the cyclic voltammogram of the anti-COVID-19 anti-body/Au microcuboid electrode after capturing 50 μL of COVID-19 protein. It illustrated two redox peaks, a cathodic peak at about 0.27 V and a. oxidation peak at about 0.45 V.

The cyclic voltammograms of different concentrations of COVID-19 protein were recorded and represented in

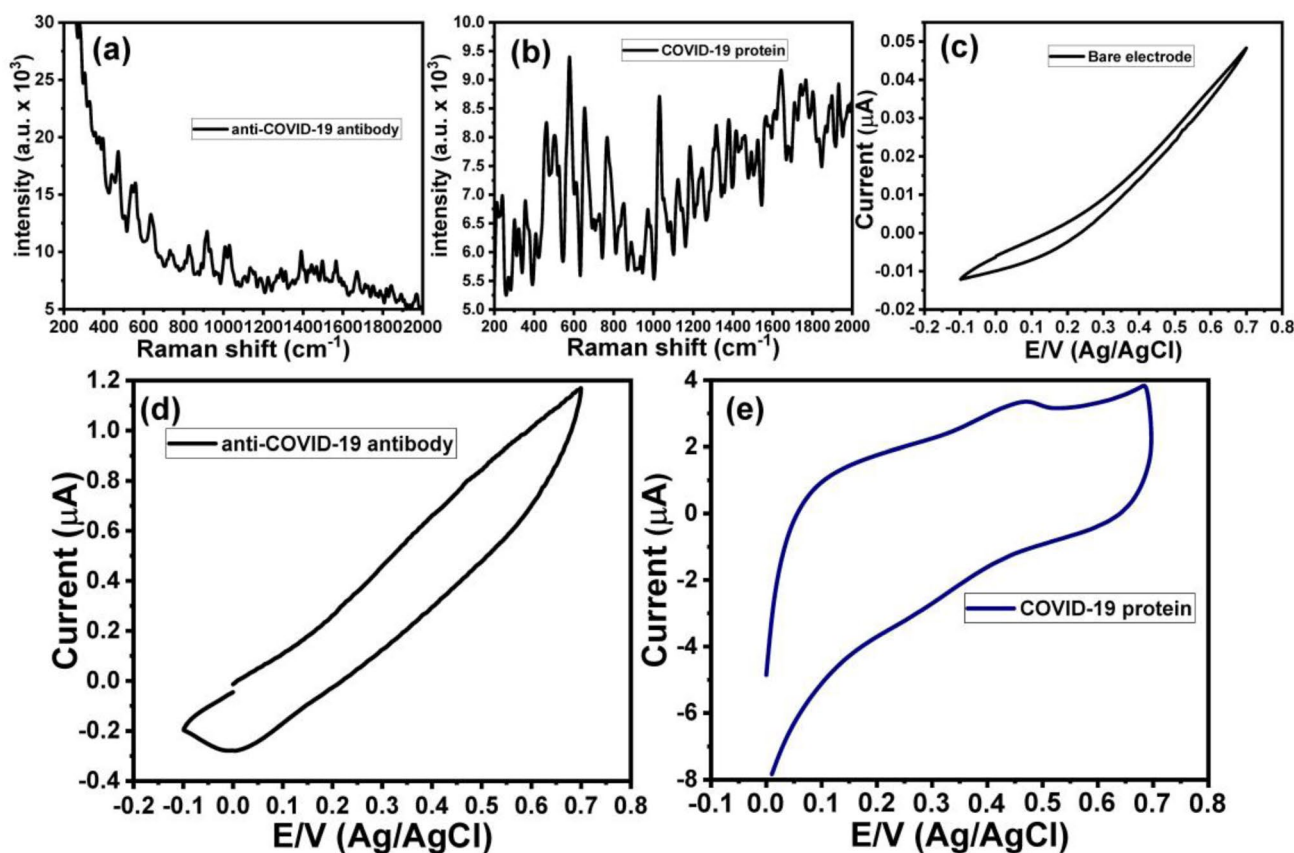


Fig. 2 a SERS spectrum of anti-COVID-19 antibody, b SERS spectra of COVID-19 protein in comparing after capturing with anti-COVID-19 antibody, c CV of bare Au microcuboid electrode, d CV

of anti-COVID-19 antibody/Au microcuboid electrode, and e CV of COVID-19 protein after interacting with anti-COVID-19 antibody/Au microcuboid electrode

Fig. 3a to investigate the efficiency of the developed sensor. The results indicated the increase of the current peak with increasing the concentration of the COVID-19 protein. Figure 3b showed the relationship between the COVID-19 protein concentrations and the current peak at about 0.45 V, which showed linear plots within a concentration range from 10 pmol L⁻¹ to 100 nmol L⁻¹ with a slope of 1.1, R^2 0.9813, and LOD of 19.5 pmol L⁻¹.

Furthermore, to develop a highly sensitive COVID-19-based sensor, we have utilized the SWV technique that is more sensitive than the CV technique. Figure 4a showed the SWV curve of the anti-COVID-19 antibody/Au microcuboid electrode within a potential window from -0.1 to 0.7 V, which almost did not show any oxidation peak. On the other hand, the SWV voltammogram of the anti-COVID-19 antibody/Au microcuboid electrode after interaction with 100 pmol L⁻¹ of COVID-19 protein showed an oxidation peak at about 0.45 V (Fig. 4b).

The effect of the scan rate on the electrochemical response of the developed sensor was studied in Fig. 4c, which shows the SWV voltammograms of 50 nmol L⁻¹ of the COVID-19 protein under different scan rates (from 10 to 100 mV/s). The results demonstrated that the redox current peaks were increased with increasing the potential scan rate; besides, the potential oxidation peak was shifted to the right side as increasing the potential scan rate. Furthermore, the relationship between the oxidation current peak and the square root of the scan rate showed a linear plot with an R^2 of 0.985 (Fig. 4d). The linear nature of the plot indicated that this system is reversible.

The efficiency of the developed sensor based on the SWV technique was also studied. Figure 5a showed the SWV voltammograms of anti-COVID-19 antibody/Au microcuboid

electrode after interacting with different concentrations of COVID-19 protein within a range from 5 pmol L⁻¹ to 100 nmol L⁻¹. The results showed an increase of the current peak as the concentration of the COVID-19 protein increased. Figure 5b illustrated the relationship between the concentrations of COVID-19 protein and the corresponding current peak at about 0.45 V that showed linear plots within this range of concentrations with a slope of 3.22 and R^2 of 0.988. The LOD of the developed sensor based on the SWV technique was found to be 276 fmol L⁻¹.

To investigate the performance of the present sensor in comparison with the previously reported COVID-19 sensor. Table 1 summarized the values of the LOD for several COVID-19 sensors based on different detecting techniques. It is worth noting that the present sensor possesses a good LOD compared to most previously reported sensors. Although some reported sensors showed lower LOD than the presented sensor, this sensor's key advantages are its simplicity and fast detection time [29–37].

2.3 Performance of the Developed Electrochemical COVID-19-Based Sensor for Monitoring COVID-19 in a Patient Sample

Finally, we have used the developed sensor for monitoring the COVID-19 in a patient sample. At first, the presence of the COVID-19 in the sample was confirmed by using the PCR technique, which indicates that this sample having the RNA gene of COVID-19. Then, we have used the developed sensor for detecting the COVID-19 based on the CV and SWV techniques. Figure 6a showed the CV response of the COVID-19 sample with the anti-COVID-19 antibody/Au microcuboid electrode, which

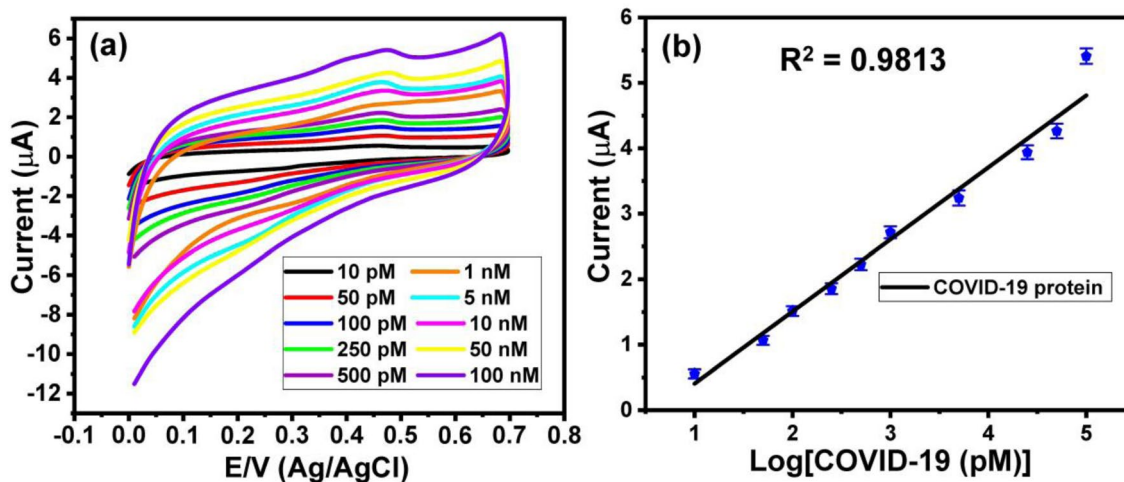


Fig. 3 a The CV of different concentrations of COVID-19 protein within a range from 100 nmol L⁻¹ to 5 pmol L⁻¹ after interacting with anti-COVID-19 antibody/Au microcuboid electrode and b the

relationship between the oxidation current peak and the concentration of COVID-19 protein

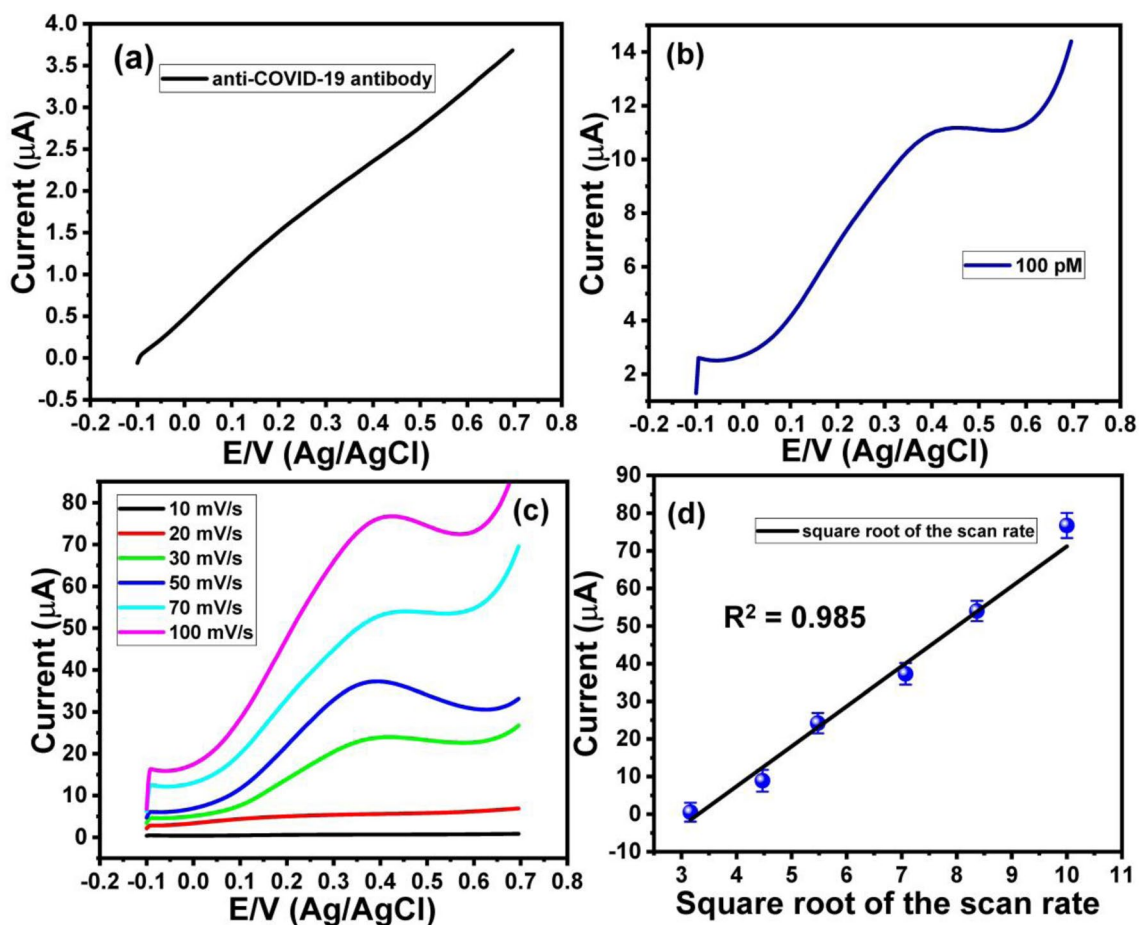


Fig. 4 **a** SWV voltammogram of anti-COVID-19 antibody/Au microcuboid electrode, **b** SWV voltammogram of COVID-19 protein after interacting with anti-COVID-19 antibody/Au microcuboid electrode, **c** the SWV voltammograms of COVID-19 protein after interacting

with anti-COVID-19 antibody/Au microcuboid electrode at different scan rate, and **d** relationship between the scan rate and the corresponding oxidation current peak

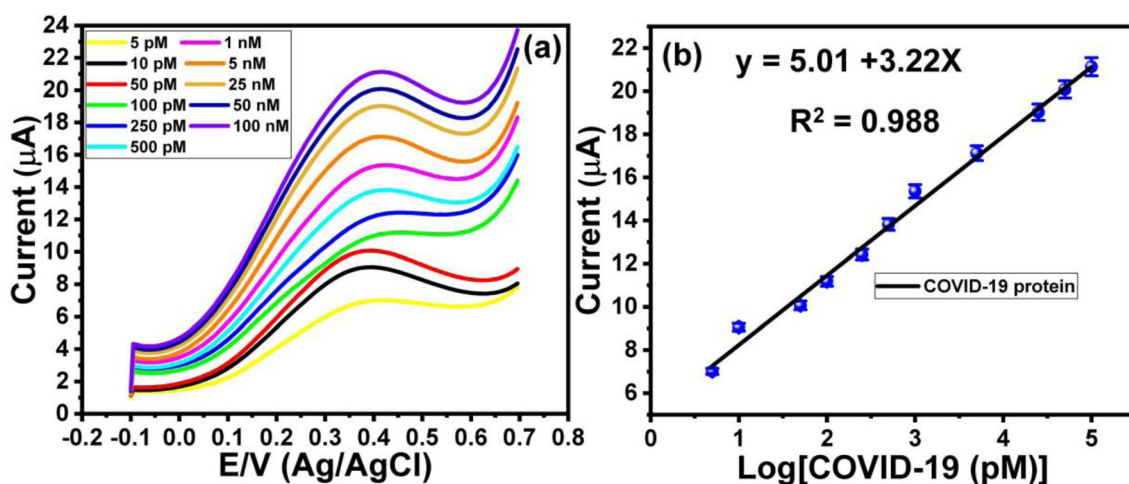


Fig. 5 **a** SWV voltammograms of different concentrations of COVID-19 protein within a range from 100 nmol L⁻¹ to 5 pmol L⁻¹ after interacting with anti-COVID-19 antibody/Au microcuboid elec-

trode and **b** the relationship between the oxidation current peak and the concentration of COVID-19 protein

Table 1 Comparison between the developed sensor and the previously reported COVID-19 sensors

Sensor	LOD	References
Glyconanoparticle platform	5 nmol L ⁻¹	[29]
Oligonucleotide capped Plasmonic nanoparticles	0.18 ng μL ⁻¹	[30]
DNA nanoscaffold hybrid chain reaction	0.96 pmol L ⁻¹	[31]
ELISA	100 ng mL ⁻¹	[32]
Quantum dot-based	10 ng mL ⁻¹	[32]
SARS-CoV-2 immunodiagnosics kit	250 pg mL ⁻¹	[33]
Electrochemical impedance spectroscopy (EIS) (Nanoprinted Reduced-Graphene-Oxide)	2.8 fmol L ⁻¹	[34]
Optical-localized surface plasmon resonance (LSPR)	2 nmol L ⁻¹	[35]
Piezoelectric immunosensor	3.5 ng mL ⁻¹	[36]
Square wave voltammetry	0.4 pg mL ⁻¹	[37]
Square wave voltammetry	276 fmol L ⁻¹	This work

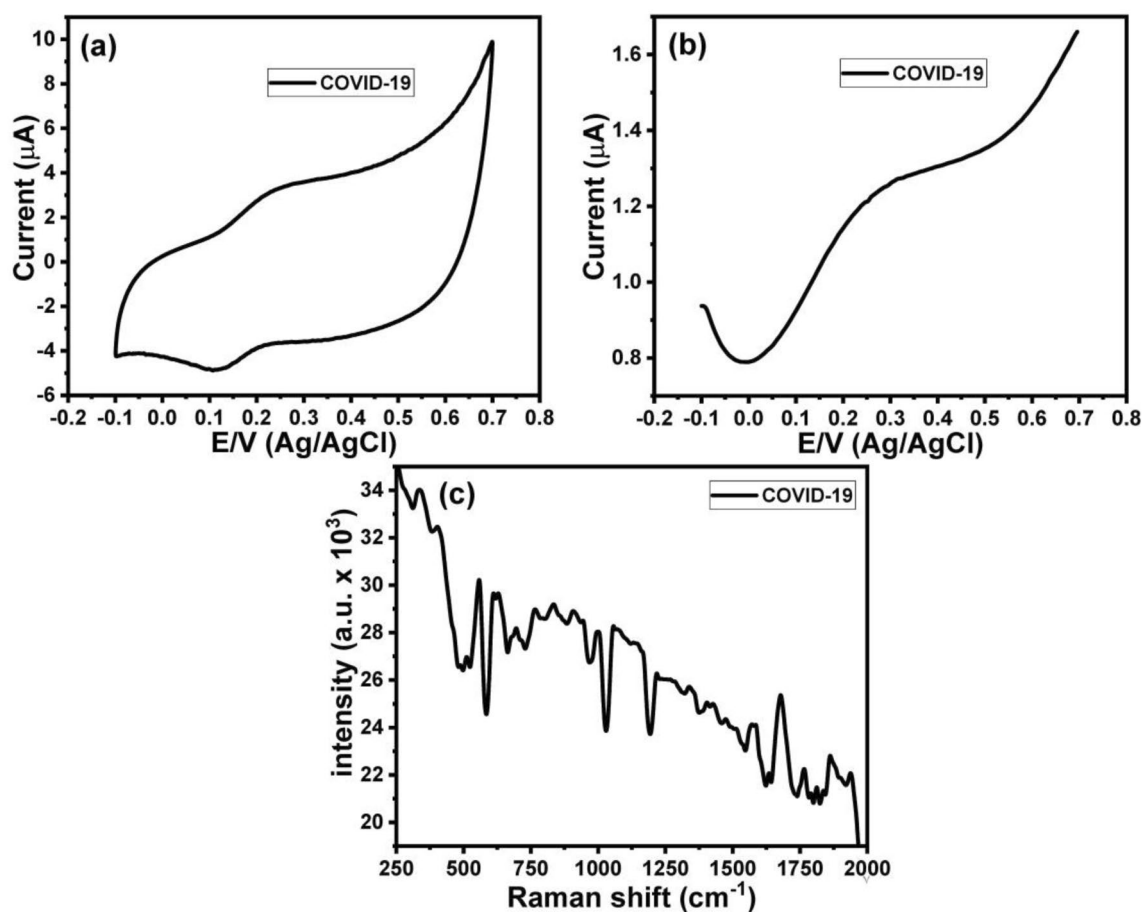


Fig. 6 **a** SERS spectra of COVID-19 protein admixed with human serum in compared with COVID-19 protein in PBS, **b** CV of COVID-19 virus after interacting with anti-antibody/Au microcuboid electrode, **c** SWV of COVID-19 virus after interacting

with anti-antibody/Au microcuboid electrode and **d** SERS spectrum of COVID-19 virus after interacting with anti-antibody/Au microcuboid electrode

showed a reversible response with an oxidation peak at about 0.3 V and a cathodic peak at 0.1 V. It is worth noting the difference between the response of the COVID-19

than COVID-19 protein because of the difference between the whole virus rather than the S protein. Furthermore, we have studied the SWV response of the COVID-19 by

using the developed sensor, which showed an oxidation peak at about 0.3 V (Fig. 6b).

To confirm the capture of the COVID-19 with the anti-COVID-19 antibody/Au microcuboid electrode, we have recorded the corresponding SERS spectrum (Fig. 6c), which exhibited a set of SERS signals, especially SERS peaks at Raman shifts of 372 cm^{-1} , $518\text{--}533\text{ cm}^{-1}$, 651 cm^{-1} , $724\text{--}838\text{ cm}^{-1}$, 936 cm^{-1} , 946 cm^{-1} , 1038 cm^{-1} , 1086 cm^{-1} , 1288 cm^{-1} , 1314 cm^{-1} , 1413 cm^{-1} , and 1596 cm^{-1} . These data showed the shifting of some besides the disappearance of the SERS peak at 290 cm^{-1} upon the presence of COVID-19 protein in the human serum. The results demonstrated the efficiency of the developed sensor for detecting the COVID-19 protein in the presence of human serum and hence the capability to detect the COVID-19 in real samples. The selectivity of the SERS technique is related to the fact that the SERS spectrum showed a unique fingerprint spectrum for each biomolecule species. The high sensitivity of the developed sensor is attributed to the uses of the Au microcuboid structures, which enhance the SERS signals of the COVID-19.

3 Conclusion

A new Au microcuboid modified PDMS was used as a flexible microelectrode and acted as a scaffold for immobilization of anti-COVID-19 antibody. Uses of the microstructures allowed the detection of a small amount of the analyte and improved the developed sensor's electrochemical conductivity. Furthermore, the interaction between the anti-COVID-19 antibody and COVID-19 protein was confirmed based on the SERS technique. Moreover, the CV and SWV techniques were used to monitor different concentrations of the COVID-19 protein that showed high efficiency to monitor COVID-19 protein with a detection limit of 276 fmol L^{-1} . Besides, we have successfully detected the COVID-19 virus in a real human sample. Thus, the developed sensor showed high sensitivity towards the COVID-19 protein and demonstrated the capability to detect COVID-19 in human samples without complicated sample preparation. One of the advantages of using this highly uniform Au nanoplate lies in using the highly uniform distribution of the micropattern with the same size and morphology that could enhance the data's reproducibility and result in quantitative data. In addition, this flexible substrate could open further applications such as chem/biosensors based on different techniques, including surface plasmon resonance, or as a SERS-active surface combined with metal nanoparticles.

4 Materials and Methods

4.1 Materials and Reagents

Au micropattern was obtained from Nanobioelectronics Laboratory (NBEL), Sogang University, Korea. PBS (pH, 7.4) was purchased from Sigma-Aldrich (St. Louis, MO, USA). COVID-19 antibody (S1N-M122, monoclonal antibody, IgG1) and COVID-19 S1 protein (S1N-C52H2, MWt = 76.9 kDa) were purchased from ACRO Biosystems (Newark, Delaware, USA). All other chemicals were analytical-grade reagents.

4.2 Fabrication of the COVID-19 Electrochemical Sensor

Figure 1 showed a schematic diagram of the development of the electrochemical COVID-19 biosensor. First, Au-coated PDMS substrates ($10\text{ mm width} \times 5\text{ mm width}$) were cleaned by rinsed with ethanol and dried under an N_2 stream. Next, a $50\text{ }\mu\text{l}$ of the antiCOVID-19 antibody ($10\text{ }\mu\text{g/ml}$) in a 10 mmol L^{-1} PBS buffer was added and kept at $4\text{ }^\circ\text{C}$ overnight. Then, we rinsed the substrates three times with 10 mmol L^{-1} PBS and dried them under nitrogen gas. Finally, $50\text{ }\mu\text{l}$ of different concentrations of COVID-19 protein concentrations in 10 mmol L^{-1} PBS were added to the substrates and incubated at $4\text{ }^\circ\text{C}$ for a further 1 h. After that, the substrate was washed three times with 10 mmol L^{-1} PBS and DIW and dried under N_2 gas. PCR was achieved using the SimpliAmp thermal cyclor (Applied Biosystems, USA). The surface morphology of the Au substrate was analyzed by a scanning electron microscope (SEM) (ISI DS-130C, Akashi Co., Tokyo, Japan) and the atomic force microscopy (AFM).

4.3 Topological Analysis by AFM

The Au substrate surface's topography was investigated with an AFM inverted optical microscope (NTEGRA spectra, NT-MDT, Russia) with a semi-contact mode at room temperature under air conditioning. The maximum scan range of the system was $100\text{ }\mu\text{m}$ in both the x and y axes. The cantilevers were NSG01 type, which had a typical resonant frequency in the range of $115\text{--}190\text{ kHz}$ and a force constant of $2.5\text{--}10\text{ N/m}$, and the images were acquired at a scan rate of 1 Hz [38].

4.4 Electrochemical Detecting of COVID-19 Concentrations

The immobilization of the anti-COVID-19 antibody and its interaction with the COVID-19 protein was confirmed using the SERES signals. The SERS spectra were collected on Raman spectroscopy with a SENTERRA inverted confocal Raman microscope (Bruker Optics Inc., Germany). A CCD camera detection system and OPUS software were employed for data acquisition. Raman spectra were recorded using NIR laser emitting light at a wavelength of 785 nm and a power of 50 mW at the sample. Ten scans of 5 s from 200 cm^{-1} to 2000 cm^{-1} were recorded, and the mean of these scans was used.

The electrochemical measurements were achieved using the AUTOLAB electrochemical workstation instrument (Metrohm, Herisau, Switzerland). We have developed a three-electrode-based homemade electrochemical cell consisting of Ag/AgCl as the reference electrode, Au microcuboid electrode as the working electrode, and Pt wire auxiliary electrode. In addition, PBS (1×, pH = 7.4) was used as the electrolyte within the potential window from -0.1 V to +0.7 V at a scan rate of 50 mV/s.

4.5 Electrochemical Sensing of COVID-19 in a Real Sample Based on CV and SWV Techniques

Here, we have used a real human sample that contains a COVID-19, which has been obtained from the nasal swab for direct detecting the COVID-19. About 50 μL of the sample was directly immobilized antiCOVID-19 antibody/Au micropattern substrate for about 6 h at room temperature. Then the substrate was directly used to investigate the COVID-19 based on CV and SWV techniques.

Acknowledgements This research is funded by King Abdulaziz City for Science and Technology (KACST), Riyadh, Saudi Arabia (Grant number: 5-20-01-031-0009). We gratefully acknowledge the financial support of the KACST.

Declarations

Conflict of interest The authors declare no competing financial interests.

References

- Liu, D.X., Liang, J.Q., Fung, T.S.: Human Coronavirus-229E, -OC43, -NL63, and -HKU1 (Coronaviridae). *Encycl. Virol.* **2**, 428–440 (2021)
- Zaki, A.M., van Boheemen, S., Bestebroer, T.M., Osterhaus, A.D.M.E., Fouchier, R.A.M.: Isolation of a novel coronavirus from a man with pneumonia in Saudi Arabia. *N. Engl. J. Med.* **367**, 1814–1820 (2012)
- World Health Organization (WHO). Middle East respiratory syndrome coronavirus (MERS-CoV), MERS situation Update November 2019. WHO; 2020. Available from: www.who.int/emergencies/mers-cov/en/ (2020).
- Ministry of Health (MOH). Command and Control Center. National Public Health Events, 2020. Ministry of Health; 2020.
- World Health Organization (WHO). MERS situation update, January 2020. Available from: <http://www.emro.who.int/pandemic-epidemic-diseases/mers-cov/mers-situation-update-january-2020.html>.
- <https://www.worldometers.info/coronavirus/>
- Huang, C., et al.: Clinical features of patients infected with 2019 novel coronavirus in Wuhan, China. *Lancet* **395**, 497–506 (2020)
- Cui, F., Zhou, H.S.: Diagnostic methods and potential portable biosensors for coronavirus disease 2019. *Biosens. Bioelectron.* **165**, 112349 (2020)
- Wu, F., et al.: A new coronavirus associated with human respiratory disease in China. *Nature* **579**, 265–269 (2020)
- Wang, D., et al.: A multiplex ELISA-based protein array for screening diagnostic proteins and diagnosis of Flaviviridae infection. *Eur. J. Clin. Microbiol. Infect. Dis.* **34**, 1327–1336 (2015)
- El-Said, W.A., Choi, J.-W.: Electrochemical biosensor consisted of conducting polymer layer on gold nanodots patterned Indium Tin Oxide electrode for rapid and simultaneous determination of purine bases. *Electrochim. Acta.* **123**, 51–57 (2014)
- Asad, M., et al.: Orange peel derived C-dots decorated CuO Nanorods for the selective monitoring of Dopamine from deboned chicken. *Electroanalysis* **32**, 11–18 (2020)
- Khalifa, M.M., et al.: Highly specific Electrochemical Sensing of *Pseudomonas aeruginosa* in patients suffering from corneal ulcers: a comparative study. *Sci. Rep.* **9**, 18320 (2019)
- Kim, T.-H., El-Said, W.A., An, J.H., Choi, J.-W.: ITO/gold nanoparticle/RGD peptide composites to enhance electrochemical signals and proliferation of human neural stem cells. *Nanomedicine* **9**, 336–344 (2013)
- El-Said, W.A., Yea, C.-H., Choi, J.-W., Kwon, I.-K.: Ultrathin polyaniline film coated on an indium-tin oxide cell-based chip for study of anticancer effect. *Thin. Solid. Films.* **518**, 661–667 (2009)
- Shin, J.-W., et al.: Silver nanoparticle modified electrode covered by graphene oxide for the enhanced electrochemical detection of dopamine. *Sensors* **17**, 2771 (2017)
- Li, R., et al.: A flexible and physically transient electrochemical sensor for real-time wireless nitric oxide monitoring. *Nat. Commun.* **11**, 3207 (2020)
- El-Said, W.A., Kim, T.-H., Chung, Y.-H., Choi, J.-W.: Fabrication of new single cell chip to monitor intracellular and extracellular redox state based on spectroelectrochemical method. *Biomaterials* **40**, 80–87 (2015)
- Senel, M., Dervisevic, M., Alhassen, S., Alachkar, A., Voelcker, N.H.: Electrochemical micropillar array-based sensor for in situ monitoring of dopamine released from neuroblastoma cells. *Anal. Chem.* **92**, 7746–7753 (2020)
- El-Said, W.A., Lee, J.-H., Oh, B.-K., Choi, J.-W.: Electrochemical sensor to detect neurotransmitter using gold nano-island coated ITO electrode. *J. Nanosci. Nanotechnol.* **11**, 6539–6543 (2011)
- El-Said, W.A., Yea, C.-H., Kwon, I.-K., Choi, J.-W.: Fabrication of electrical cell chip for the detection of anticancer drugs and environmental toxicants effect. *BioChip. J.* **3**, 105–112 (2009)
- Abbas, Y., et al.: Heteroatom-doped Carbon nanoparticle-ionic liquid composites as electrochemical sensors for Uric acid. *ACS. Appl. Nano. Mater* **3**, 11383–11390 (2020)

23. Yilmaz, D., et al.: Application of Raman spectroscopy in monoclonal antibody producing continuous systems for downstream process intensification. *Biotechnol. Prog.* **36**, e2947 (2020)
24. Wen, Z.-Q.: Raman spectroscopy of protein pharmaceuticals. *J. Pharm. Sci.* **96**, 2861–2878 (2007)
25. Ashton, L., Blanch, E.W.: pH-induced conformational transitions in α -lactalbumin investigated with two-dimensional Raman correlation variance plots and moving windows. *J. Mol. Struct.* **974**, 132–138 (2010)
26. McAvan, B.S., et al.: Raman spectroscopy to monitor post-translational modifications and degradation in Monoclonal antibody therapeutics. *Anal. Chem.* **92**, 10381–10389 (2020)
27. Baker, A.E., Mantz, A.R., Chiu, M.L.: Raman spectroscopy characterization of antibody phases in serum. *mAbs* **6**, 1509–1517 (2014)
28. Ettah, I., Ashton, L.: Engaging with Raman spectroscopy to investigate antibody aggregation. *Antibodies* **7**, 24 (2018)
29. Baker, A.N., et al.: The SARS-COV-2 spike protein binds sialic acids and enables rapid detection in a lateral flow point of care diagnostic device. *ACS. Cent. Sci.* **6**, 2046–2052 (2020)
30. Moitra, P., Alafeef, M., Dighe, K., Frieman, M., Pan, D.: Selective naked-eye detection of SARS-CoV-2 mediated by N gene targeted antisense oligonucleotide capped plasmonic nanoparticles. *ACS. Nano.* **14**, 7617–7627 (2020)
31. Jiao, J., et al.: DNA nanoscaffold-based SARS-CoV-2 detection for COVID-19 diagnosis. *Biosens Bioelectron* **167**, 112479 (2020)
32. Ji, T., et al.: Detection of COVID-19: a review of the current literature and future perspectives. *Biosens Bioelectron* **166**, 112455 (2020)
33. Mertens, P., et al.: Development and potential usefulness of the COVID-19 Ag Respi-Strip diagnostic assay in a pandemic context. *Front. Med.* **7**, 225 (2020)
34. Ali, Md.A., et al.: Sensing of COVID-19 antibodies in seconds via Aerosol Jet Nanoprinted reduced-Graphene-oxide-coated 3D electrodes. *Adv. Mater.* **33**, 2006647 (2021)
35. Shi, L., et al.: Development of SPR biosensor for simultaneous detection of multiplex respiratory viruses. *Biomed. Mater. Eng.* **26**, S2207–S2216 (2015)
36. Lee, T., et al.: Recent advances in AIV biosensors composed of Nanobio hybrid material. *Micromachines* **9**, 651 (2018)
37. Layqah, L.A., Eissa, S.: An electrochemical immunosensor for the corona virus associated with the Middle East respiratory syndrome using an array of gold nanoparticle-modified carbon electrodes. *Microchim. Acta.* **186**, 224 (2019)
38. El-Said, W.A., Yea, C.-H., Jung, M., Kim, H., Choi, J.-W.: Analysis of effect of nanoporous alumina substrate coated with polypyrrole nanowire on cell morphology based on AFM topography. *Ultramicroscopy* **110**(6), 676 (2010)

Publisher's Note Springer Nature remains neutral with regard to jurisdictional claims in published maps and institutional affiliations.